J. Astrophys. Astr. (2022) 43:87
https://doi.org/10.1007/s12036-022-09866-z

TRANSIENTS

Analyses of hydrogen-stripped core–collapse supernovae using MOSFiT and MESA-based tools

AMAR ARYAN[1,2,*], SHASHI BHUSHAN PANDEY[1], AMIT KUMAR[1,3], RAHUL GUPTA[1,2], AMIT KUMAR ROR[1], APARA TRIPATHI[2] and SUGRIVA NATH TIWARI[2]

[1]Aryabhatta Research Institute of Observational Sciences (ARIES), Nainital 263001, India.
[2]Department of Physics, Deen Dayal Upadhyaya Gorakhpur University, Gorakhpur 273009, India.
[3]School of Studies in Physics and Astrophysics, Pt. Ravishankar Shukla University, Chattisgarh 492010, India.
*Corresponding author. E-mails: amararyan941@gmail.com; amar@aries.res.in

MS received 2 December 2021; accepted 31 May 2022

Abstract. In this work, we employ two publicly available analysis tools to study four hydrogen (H)–stripped core–collapse supernovae (CCSNe), namely, SN 2009jf, iPTF13bvn, SN 2015ap and SN 2016bau. We use the modular open-source fitter for transients (`MOSFiT`) to model the multi-band light curves. `MOSFiT` analyses show ejecta masses (log M_{ej}) of $0.80^{+0.18}_{-0.13}$ $M_{\odot}$, $0.15^{+0.13}_{-0.09}$ $M_{\odot}$, $0.19^{+0.03}_{-0.03}$ $M_{\odot}$ and $0.19^{-0.01}_{+0.02}$ $M_{\odot}$ for SN 2009jf, iPTF13vn, SN 2015ap and SN 2016au, respectively. Later, modules for experiments in stellar astrophysics (`MESA`), is used to construct models of stars from pre-main sequence upto core collapse, which serve as the possible progenitors of these H-stripped CCSNe. Based on literature, we model a 12 $M_{\odot}$ ZAMS star as the possible progenitor for iPTF13vn, SN 2015ap and SN 2016bau, while a 20 $M_{\odot}$ ZAMS star is modeled as the possible progenitor for SN 2009jf. Glimpses of stellar engineering and physical properties of models at various stages of their lifetime have been presented to demonstrate the usefulness of these analysis threads to understand the observed properties of several classes of transients in detail.

Keywords. Supernovae—MOSFiT—`MESA`.

1. Introduction

Core–collapse Supernovae (CCSNe) are extremely powerful explosions that mark the death of massive stars, further sub-divided into various classes subjected to the presence/absence of H in their photospheric phase spectra (Filippenko 1988; Filippenko *et al.* 1993; Smartt 2009; Maoz *et al.* 2014; Van Rossum *et al.* 2016; Könyves-Tóth *et al.* 2020). Among H-deficient ones, near peak, the type Ib SNe exhibit prominent helium (He)-features in their spectra, whereas type Ic SNe show neither H nor He obvious features. Prominent features of intermediate-mass elements, such as O, Mg and Ca are also seen in type Ib and type Ic SNe spectra. Another very interesting class, known as type IIb SNe form a transition class of objects that are supposed to link SNe II and SNe Ib (Filippenko 1988; Filippenko *et al.* 1993; Smartt 2009). The early-phase spectra of SNe IIb display prominent H-features, while unambiguous He-features appear after a few weeks (Filippenko 1997). The CCSNe are the final destinations of massive stars ($\gtrsim$8–10 $M_{\odot}$; e.g., Garry 2004; Woosley & Janka 2005; Groh 2017), resulting from the core–collapse due to the exhaustion of the nuclear fuel in their cores.

Underlying physical mechanisms behind above-mentioned classes of CCSNe, are still not understood well. One popular mechanism is the neutrino-driven outflow (Muller 2017 and references therein), but other mechanisms have also been proposed (e.g., magneto-rotational mechanism of the explosion of CCSNe as discussed in Bisnovatyi-Kogan *et al.* (2018)). In many cases, the CCSNe explosions are not spherically symmetrical. As a particular case, studies by Couch *et al.* (2009) indicate that the aspherical CCSNe from red

This article is part of the Special Issue on "Astrophysical Jets and Observational Facilities: A National Perspective".

Published online: 19 November 2022

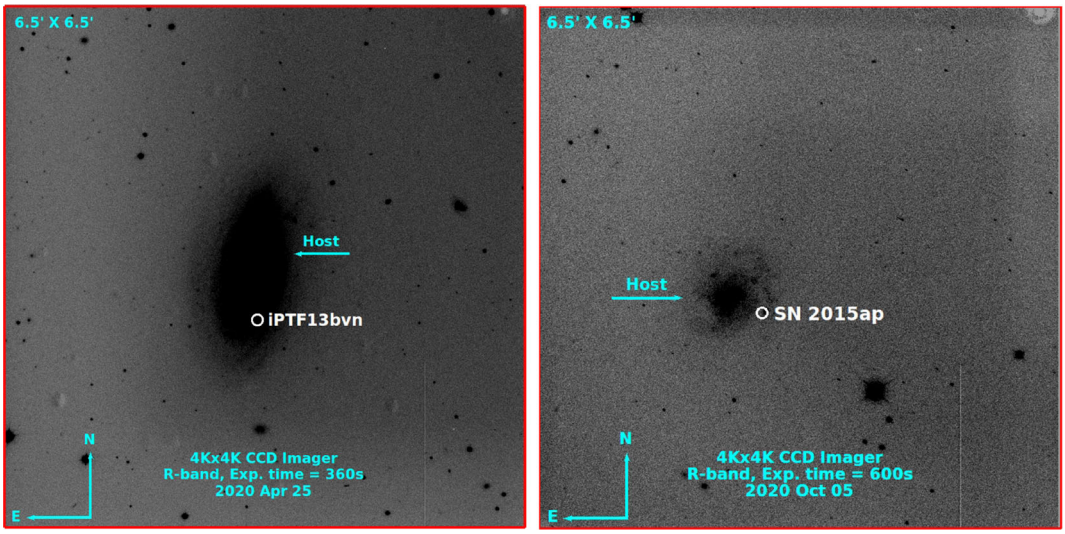

Figure 1. Finding charts of iPTF13bvn and SN 2015ap host galaxies in R-band using the 4K×4K CCD imager (Pandey & Yadav 2018; Kumar *et al.* 2021) mounted at the axial port of the 3.6m DOT in the left and right panels, respectively, are shown to demonstrate a diverse set of environments and locations within the host galaxies.

supergiants, are powered by non-relativistic Jets. Further, (Piran *et al.* 2019 and references therein) mention that gamma-ray bursts (GRBs) that accompany rare and powerful CCSNe (popularly known as 'hypernovae') involve the association of relativistic jets emerging due to the explosion of a certain class of massive stars exploding under specific physical conditions.

During the last stages of their lives, the stars are fully evolved and contain mostly intermediate (e.g., Si, Mg, etc.) to high mass elements (e.g., Fe, Ni, Co, etc.) through various nuclear processes. So, stellar deaths through these catastrophic events are also responsible for the chemical enrichment of our universe apart from the birth of compact objects like neutron stars and black holes alone. Nuclear astrophysics aims at understanding the nuclear processes that take place in the universe. These nuclear processes generate energy in stars and contribute to the nucleosynthesis of the elements and the evolution of galaxy through many possible channels including SN explosions. The collapses of the stellar cores produce elements through various possible ways (e.g., s/r/p processes), enriching interstellar medium. This research field has now evolved as a developed one (e.g., Liccardo *et al.* 2018; Meyer *et al.* 2020 and references therein) demanding a multi-wavelength study to better understand not only the nuclear processes, but also the nature of the possible progenitors behind such cosmic explosions. It is now known that a good fraction of well-studied H-stripped CCSNe happen in diverse types of host galaxies (Figure 1) having a range of physical properties like mass, luminosity, age, star formation rates, etc. Late time observations of these host galaxies are of crucial importance to decipher the nature of possible progenitors exploding in a diverse range of environments. Apart from multi-band observations of these events, detailed studies about ambient media of such host galaxies and their pre-explosion images are very useful to constrain the nature of possible progenitors.

In the light of above and the published work earlier, as part of the present analysis, we chose a sample of 4 H-stripped CCSNe (i.e., SN 2009jf (Sahu *et al.* 2011; Valenti *et al.* 2011), iPTF13bvn (Cao *et al.* 2013; Bersten *et al.* 2014; Eldridge *et al.* 2015), SN 2015ap (Aryan *et al.* 2021a) and SN 2016bau (Aryan *et al.* 2021a)) to fit their multi-band optical light curves using `MOSFiT` (Guillochon *et al.* 2018). Further, the fitting parameters obtained using `MOSFiT` are used to characterize the nature of possible progenitors using 1-D hydrodynamical modeling code `MESA` (Paxton *et al.* 2011, 2013, 2015, 2018, 2019). All the analyses performed in this work, made use of publicly available tools. More details about the usefulness of analysis tools like `MESA/MOSFiT` (and others) are described in (Aryan *et al.* 2021b, 2022a, among many others) depicting how these tools can be boon to the transient community.

This paper has been divided into five sections. A brief introduction and methods to fit the light curves of various SNe have been presented in Section 2. In Section 3, the basic assumptions and various physical and chemical properties of the possible progenitors of different SNe have been presented. We discuss the major

Table 1. Adopted total-extinction values ($E(B-V)_{\rm tot}$), adopted luminosity distances (D_L) and redshift (z) of SNe considered in the present analysis.

SN name	$E(B-V)_{\rm tot}$ (mag)	D_L (Mpc)	Redshift
SN 2009jf	0.112 (Sahu *et al.* 2011)	34.66 (Sahu *et al.* 2011)	0.007942 (Sahu *et al.* 2011)
iPTF13bvn	0.21 (Bersten *et al.* 2014)	25.8 (Bersten *et al.* 2014)	0.00449 (Cao *et al.* 2013)
SN 2015ap	0.037 (Prentice *et al.* 2019; (Aryan *et al.* 2021a)	46.6 (Aryan *et al.* 2021a)	0.01138 (Aryan *et al.* 2021a)
SN 2016bau	0.579 (Aryan *et al.* 2021a)	21.77 (Aryan *et al.* 2021a)	0.003856 (Aryan *et al.* 2021a)

outcomes of our studies in Section 4 and provide our concluding remarks in Section 5.

2. Fitting light curves using MOSFiT

MOSFiT is a Python-based package that downloads data from openly available online catalogs, generates the Monte Carlo ensembles of semi-analytical light-curve fits to downloaded data sets along with their associated Bayesian parameter posteriors and provides the fitting results back. Besides fitting data downloaded from openly available online catalogs, one can also perform a similar analysis to the private data sets. MOSFiT employs various powering mechanisms for the light curves of different types of SNe. Some of them are: (a) default model incorporating the nickel–cobalt decay (Nadyozhin 1994), (b) magnetar model that takes a magnetar engine with simple spectral energy distribution (Nicholl *et al.* 2017) and (c) csm model which are interacting CSM–SNe (Chatzopoulos *et al.* 2013; Villar *et al.* 2017). A detailed description of all the models available through MOSFiT is provided in Guillochon *et al.* (2018).

In this work, we tried to fit the multi-band light curves of four type Ib SNe. These four SNe are SN 2009jf, iPTF13bvn, SN 2009jf and SN 2016bau. We employ the default model to fit the multi-band light curves of these SNe. The multi-band light curves of SN 2009jf and iPTF13bvn have been taken from Sahu *et al.* (2011) and Bersten *et al.* (2014), respectively, while the source of multi-band light curves of SN 2015ap and SN 2016bau is Aryan *et al.* (2021a). Further, total extinction ($E(B-V)_{\rm tot}$), luminosity distance (D_L) and redshift (z) of each SN in the present study are given in Table 1.

The MOSFiT calculations for all other four SNe were already performed in Meyer *et al.* (2020), but in their study, Meyer *et al.* (2020) simply fit the data available from open supernova catalog (Guillochon *et al.* 2017). Previous studies and fits performed from the data directly imported from open supernova catalog, lack a few corrections including host galaxy extinction correction, etc. Also, sometimes only a few data points are available to fit from open supernova catalog similar to the cases like SN 2015ap and SN 2016bau in Meyer *et al.* (2020). However, in the present analysis, the data for each SN are taken from the referenced sources, corrected for total (milky way and host galaxy) extinction and then, privately fit using MOSFiT using a larger data set. Thus, we consider our fittings using MOSFiT to be more reliable, and thus, fitting parameters obtained through our analyses are better.

For SN2009jf, MOSFiT fittings give an ejecta mass of (M_{ej}) $\sim 6.31\ M_{\odot}$, which is in very good agreement with Sahu *et al.* (2011) and Valenti *et al.* (2011), while Meyer *et al.* (2020) underpredicts the M_{ej} ($\sim$2.45 $M_{\odot}$). Further, for iPTF13bvn, we obtain $M_{ej} \sim 1.41\ M_{\odot}$, agreeing closely with Eldridge *et al.* (2015) and Paxton *et al.* (2019), while Meyer *et al.* (2020), once again underpredicts the M_{ej}. Similarly, for SN 2015ap and SN 2016bau, we obtain ejecta masses of $\sim$1.54 $M_{\odot}$ and 1.54 $M_{\odot}$, respectively. The M_{ej} from our MOSFiT fittings for SN 2015ap is close to Prentice *et al.* (2019), but lower than what is obtained from Aryan *et al.* (2021a). For SN 2015ap, Meyer *et al.* (2020) also produced similar value of M_{ej}. The M_{ej} from our MOSFiT fittings for SN 2016bau are very close to Aryan *et al.* (2021a) while Meyer *et al.* (2020) predicts much lower value.

Figure 2 shows the results of fitting default model using MOSFiT to the multi-band light curves of SN 2009jf, iPTF13bvn, SN 2015ap and SN 2016bau. The corner plot of the fitting parameters of the default model for SN 2015ap has been shown in Figure 3 as an example. Similar corner plots are generated for other SNe also. The fitting parameters of the default model to other four SNe are listed in Table 2.

3. Understanding the possible progenitors of sub-sample of CCSNe using MESA

MESA (version r11701) is a one-dimensional stellar evolution code. It is open source, rich, efficient having thread-safe libraries for a wide range of applications in computational stellar astrophysics. The capacity of MESA is enormous. It can be used to study various

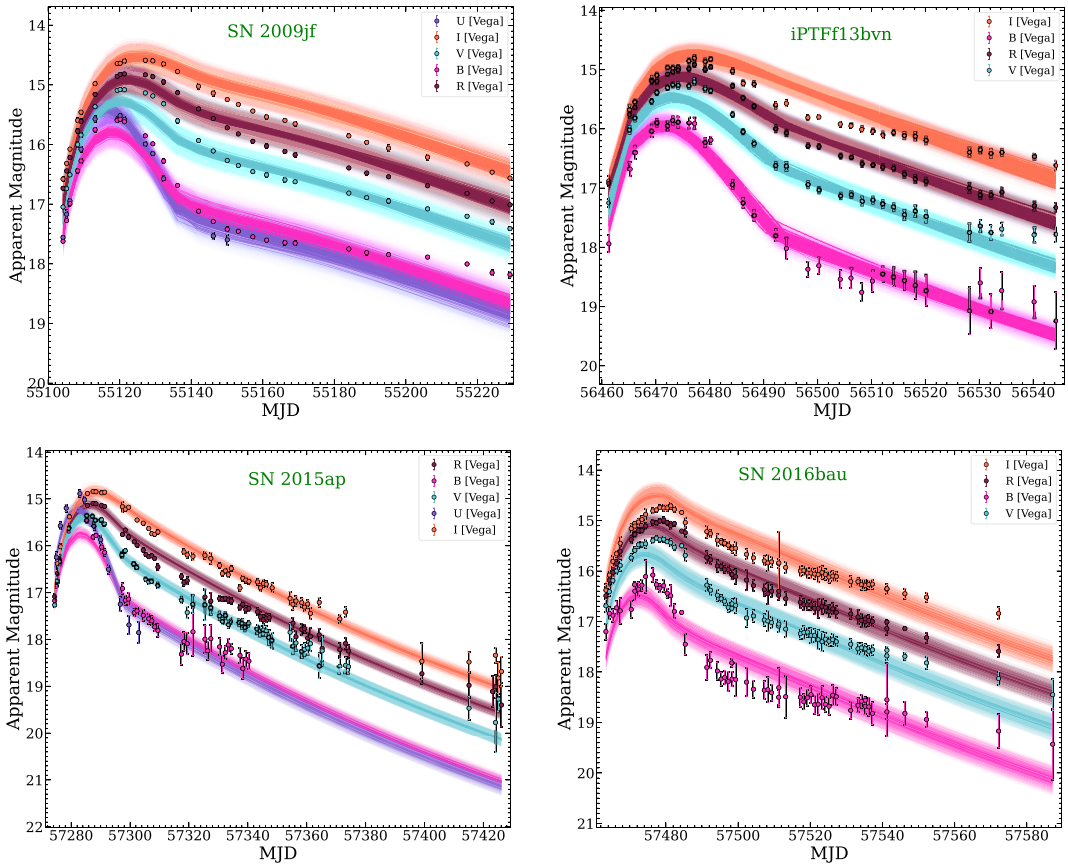

Figure 2. Results of `MOSFiT` fittings to the multi-band light curves of SN 2009jf, iPTF13bvn, SN 2015ap and SN 2016bau, respectively. For type Ib SNe, the radioactive decay of ^{56}Ni and ^{56}Co is considered to be the prominent powering mechanism for their light curves. Thus, the `default` model from `MOSFiT` has been employed to fit the light curves of these SNe.

phases of stellar evolution resulting in various types of SNe, pulsations in stars, accretion onto a neutron star, black hole formations and many other astrophysical phenomena. Following Cao *et al.* (2013), Sahu *et al.* (2011) and Aryan *et al.* (2021a) iPTF13bvn, SN 2015ap, SN 2016bau and SN 2009jf have progenitors with ZAMS masses in the range of 11–20 $M_{\odot}$. In this work, following Aryan et al. (2021a; 2022b) and Pandey *et al.* (2021), we attempt to understand the physical and chemical properties of 12 $M_{\odot}$ and 20 $M_{\odot}$ ZAMS stars which could be the possible ZAMS mass range for the progenitors of these SNe. We briefly mention the `MESA` settings and assumptions for our calculations below.

For the 12 $M_{\odot}$ ZAMS progenitor model that could be the progenitor of iPTF13bvn, SN 2015ap or SN 2016bau (from Cao *et al.* (2013) and Aryan *et al.* (2021a)), our calculations closely follow Aryan *et al.* (2021a). A brief description of the 12 $M_{\odot}$ ZAMS progenitor model has been provided. Starting from the pre-main-sequence (PMS), the 12 $M_{\odot}$ ZAMS star is evolved through various stages on the HR diagram until the onset of core–collapse. We consider rotationless progenitor having an initial metallicity of $Z = 0.02$, because these three SNe prove to be arising in the regions, having metallicities close to solar metallicity. The convection is modeled using the mixing theory of Henyey *et al.* (1965) by adopting the Ledoux criterion. The mixing-length parameter is set to $\alpha = 3.0$ in the region, where the mass fraction of hydrogen is >0.5, and $\alpha = 1.5$ for the other regions. Further, the semi-convection is modeled following Langer *et al.* (1985) having an efficiency parameter of $\alpha_{\rm sc} = 0.01$. For the thermohaline mixing, following Kippenhahn *et al.* (1980), the efficiency parameter is set as $\alpha_{\rm th} = 2.0$. The convective overshooting is modeled using the diffusive approach of Herwig (2000), with $f = 0.01$ and $f_0 = 0.004$ for all the convective core and shells. For the stellar wind, `Dutch` scheme is used with a scaling factor of 1.0. We employed satisfactory spatial and temporal resolution in our models by choosing `mesh_delta_coeff` = 1.0 and `varcontrol_target` = 5d-4.

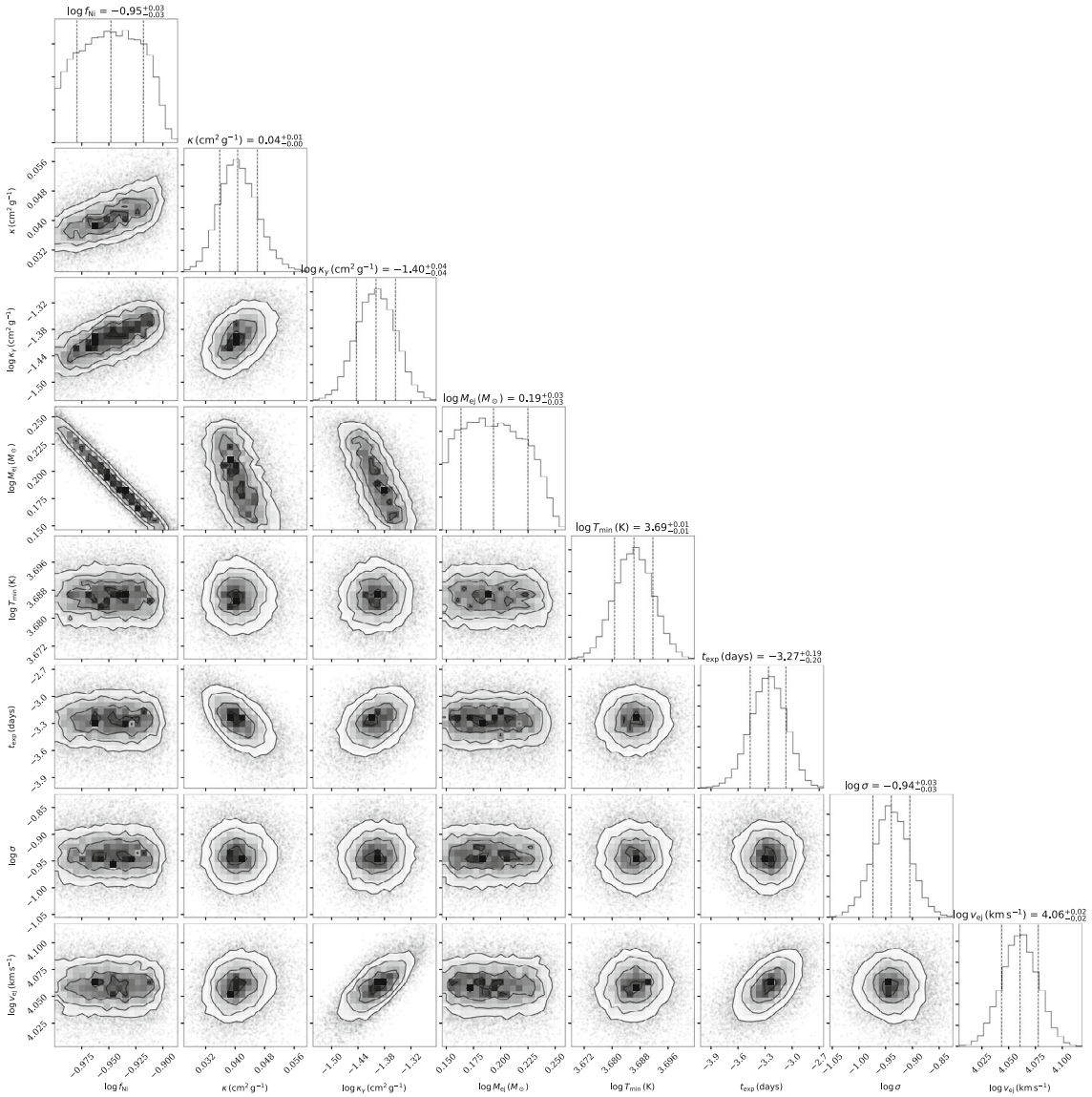

Figure 3. Corner plot of the fitting parameters from the `default` model for SN 2015ap using `MOSFiT`.

For the 20 $M_\odot$ ZAMS progenitor model, similar settings have been used including an initial metallicity of $Z = 0.02$. SN 2009jf occurred in a region having metallicity close to the solar metallicity, thus $Z = 0.02$ is used for the 20 $M_\odot$ model too, serving as the possible progenitor of SN 2009jf. A slightly better spatial resolution is employed by taking `mesh_delta_coeff` $= 0.8$.

Figure 4 shows the evolutions of the 12 $M_\odot$ and 20 $M_\odot$ ZAMS progenitors on the HR diagram starting from PMS to the exhaustion of He-burning in the core. At the end of the core He-burning phase, both models are living in the red-giant/supergiant phase. Figures 5 and 6 show the snapshots of the chemical compositions of the progenitor stars at two phases each. The left panels of Figures 5 and 6 show the stellar compositions when the models have just landed on the ZAMS, while their right panels show the chemical composition of models until the end of the core He-burning.The grey circles in each subplot indicate the location of the mass coordinates at 0.25, 0.5. 0.75 and 1.00 times the total stellar mass. It can be noticed that initially (depending on the metallicity), the fraction of H and He are much higher than other heavy metals, but as the models evolve and reach the end of the He-burning in the core, the composition of heavier elements increases in the core. Other important noticeable properties

Table 2. Best-fit parameters and 68% uncertainties for the `default` model. The parameters for the source with ∗ are the results from Meyer *et al.* (2020) presented here for comparison with our studies. In this table, M_{ej} is the ejecta mass, f_{Ni} is the Nickel mass fraction, κ is the Thomson electron scattering opacity, κ_γ is gamma-ray opacity of the SN ejecta, v_{ej} represents the ejecta velocity, $T_{\rm min}$ is an additional parameter for temperature floor (see Nicholl *et al.* (2017) for further details), σ is an additional variance parameter, which is added to each uncertainty of the measured magnitude so that the reduced χ^2 approaches 1 and $t_{\rm exp}$ is the epoch of explosion since first detection

Source name	$\log M_{\rm ej}$ ($M_\odot$)	$\log f_{\rm Ni}$	κ (cm^2 g^{-1})	$\log \kappa_\gamma$ (cm^2 g^{-1})	$\log v_{\rm ej}$ (km s^{-1})	$\log T_{\rm min}$ (K)	$\log \sigma$	$t_{\rm exp}$ (days)
SN2009jf	$0.80^{+0.18}_{-0.13}$	$-1.47^{-0.18}_{+0.13}$	$0.03^{+0.01}_{-0.01}$	$-1.60^{+0.14}_{-0.18}$	$3.93^{+0.03}_{-0.03}$	$3.69^{+0.01}_{-0.01}$	$-0.65^{-0.03}_{+0.03}$	$-4.65^{-0.33}_{+0.30}$
SN2009jf*	$0.39^{+0.19}_{-0.12}$	$-1.14^{-0.20}_{+0.11}$	$0.13^{+0.04}_{-0.04}$	$1.60^{+1.52}_{-1.64}$	$3.95^{+0.02}_{-0.02}$	$3.61^{+0.01}_{-0.01}$	$-0.77^{-0.03}_{+0.04}$	$-4.53^{-0.23}_{+0.20}$
iPTF13bvn	$0.15^{+0.13}_{-0.09}$	$-1.12^{+0.09}_{-0.13}$	$0.04^{+0.01}_{-0.01}$	$-1.77^{+0.11}_{-0.13}$	$3.83^{+0.02}_{-0.02}$	$3.65^{+0.01}_{-0.01}$	$-0.74^{-0.03}_{+0.03}$	$-3.85^{-0.30}_{+0.28}$
iPTF13bvn*	$-0.04^{+0.21}_{-0.12}$	$-1.36^{-0.18}_{+0.14}$	$0.12^{+0.05}_{-0.04}$	$1.55^{+1.54}_{-1.62}$	$3.82^{+0.01}_{-0.01}$	$3.56^{+0.00}_{-0.01}$	$-0.66^{-0.02}_{+0.02}$	$-1.92^{-0.08}_{+0.07}$
SN2015ap	$0.19^{+0.03}_{-0.03}$	$-0.95^{-0.03}_{+0.03}$	$0.04^{+0.01}_{-0.00}$	$-1.40^{+0.04}_{-0.04}$	$4.06^{+0.02}_{-0.02}$	$3.69^{+0.01}_{-0.01}$	$-0.94^{-0.03}_{+0.03}$	$-3.27^{-0.20}_{+0.19}$
SN2015ap*	$0.25^{+0.16}_{-0.12}$	$-0.24^{-0.22}_{+0.15}$	$0.10^{+0.05}_{-0.03}$	$1.73^{+1.48}_{-1.58}$	$4.45^{+0.03}_{-0.03}$	$3.41^{+0.24}_{-0.25}$	$-0.80^{-0.05}_{+0.07}$	$-3.64^{-0.40}_{+0.29}$
SN2016bau	$0.19^{-0.01}_{+0.02}$	$-0.94^{-0.02}_{+0.02}$	$0.05^{+0.00}_{-0.00}$	$-1.46^{+0.06}_{-0.06}$	$3.95^{+0.02}_{-0.02}$	$3.82^{+0.01}_{-0.01}$	$-0.65^{-0.02}_{+0.02}$	$-4.88^{-0.06}_{+0.14}$
SN2016bau*	$-0.51^{-0.18}_{+0.23}$	$-1.01^{-0.25}_{+0.21}$	$0.10^{+0.04}_{-0.03}$	$2.45^{-2.48}_{-3.41}$	$3.58^{+0.14}_{-0.02}$	$3.55^{+0.31}_{-0.38}$	$-1.72^{-0.18}_{+0.23}$	$-4.41^{-0.36}_{+0.29}$

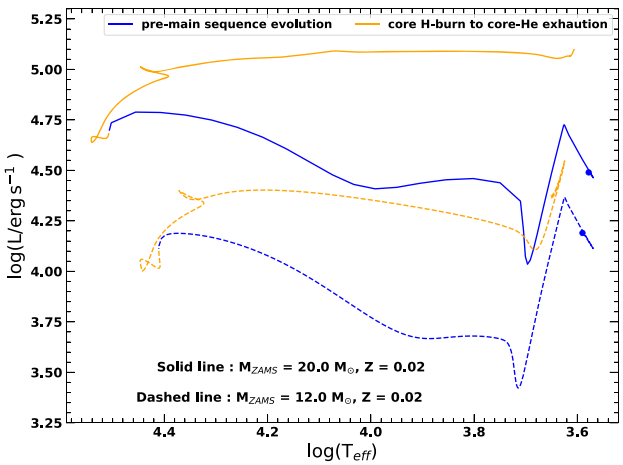

Figure 4. Evolutions of 12 $M_\odot$ and 20 $M_\odot$ models (both having $Z = 0.02$) on HR diagram from PMS till the exhaustion of He-burning in their core. The blue solid circles mark the beginning of PMS evolution of the two models.

include the significant stripping of envelope due to the presence of stellar wind as the models evolve. The 12 $M_\odot$ progenitor model has lost around 1 $M_\odot$ as it reaches the termination stage of core-He burning, while at the similar stage, the 20 $M_\odot$ progenitor model has lost a significant amount of envelope retaining 15.1 $M_\odot$ (i.e., lost around 4.9 $M_\odot$ of its outer envelope) of total ZAMS mass. The high mass loss in the case of 20 $M_\odot$ progenitor model could be attributed to the presence of comparatively stronger stellar winds than in the case of 12 $M_\odot$ model.

The SNe considered in this study are all type Ib. SNe Ib have been considered to originate from massive stars which lose almost all of their hydrogen envelope, most probably due to binary interaction (e.g., Yoon *et al.* 2010; Dessart *et al.* 2012; Eldridge & Maund 2016) or due to strong stellar winds (e.g., Gaskell *et al.* 1986; Eldridge *et al.* 2011; Groh *et al.* 2013). Here, to produce such a stripped model, the hydrogen envelopes are artificially stripped. Specifically, after evolving the model until the exhaustion of helium, an artificial mass-loss rate of $\dot{M} \gtrsim 10^{-4}\ M_\odot\ {\rm yr}^{-1}$ has been imposed until the total hydrogen masses of the models go down to 0.01 $M_\odot$. After the hydrogen masses in the models reach the specified limit, the artificial mass loss is switched off and the models are further evolved on the HR diagram until the onset of the core–collapse. Starting from 12 $M_\odot$ at ZAMS, our model has a total mass of 3.42 $M_\odot$ at an stage just before the core–collapse. For the 20 $M_\odot$ ZAMS progenitor, the model has a total mass of around 6.50 $M_\odot$ just before the core–collapse.

Thus, after approaching the ZAMS sequence, our models evolve to become giants/supergiants. Further, they suffer stripping and evolve ahead to start Si-burning in their respective cores. As a result, our models develop inert Fe-cores that result in the core–collapse due to the absence of any further fusion processes in the core. Figure 7 shows the variation of core temperature ($T_{\rm core}$) with the core density ($\rho_{\rm core}$) as the models evolve from PMS until the onset of their core–collapses. In the last evolutionary phases, the $T_{\rm core}$ and $\rho_{\rm core}$ reach in excess

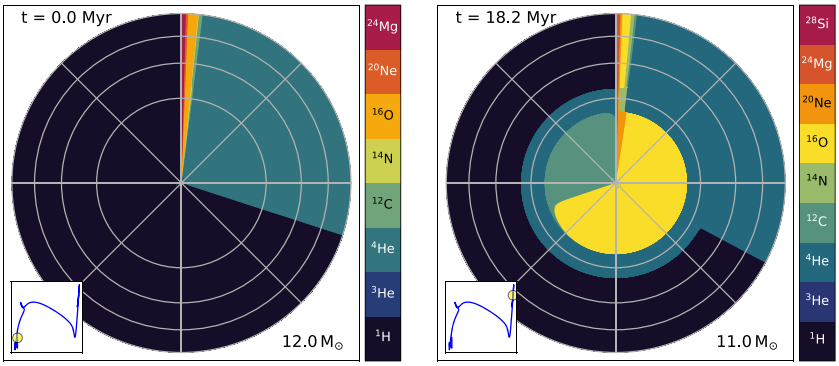

Figure 5. Abundances of various elements in the stellar interior of the 12 $M_\odot$ progenitor with $Z = 0.02$, at two stages. Left: The abundances of various elements when the model has just arrived on the main-sequence. Right: The abundances of various elements as the model has finished core-He burning. The compositions of heavier elements in the stellar interior have increased now.

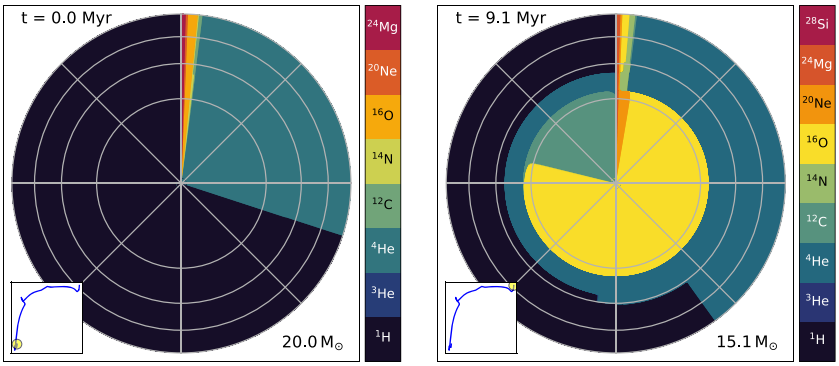

Figure 6. Abundances of various elements in the stellar interior of the 20 $M_\odot$ progenitor with $Z = 0.02$ at two stages. Left: The abundances of various elements when the model has just arrived on the main-sequence. Right: The abundances of various elements as the model has finished core-He burning. Similar to 12 $M_\odot$ model, the compositions of heavier elements have increased now.

of 10^{10} K and 10^{10} g cm^{-3}, respectively. Such high central temperatures and densities are considered to be the suitable physical conditions for the stellar core to collapse.

Further, Figure 8 shows the mass fractions of various elements present inside the model stars when their cores are about to collapse. Near the surface of the stellar models, the fraction of He is much higher compared to other elements. Such high mass fractions of He near the surface of progenitors just before the core–collapse is responsible for the type Ib SNe displaying strong He-features in their spectra. As we move inwards, towards the center of the stellar models, the cores consist mainly inert ^{56}Fe, responsible for the cores to collapse.

4. Results and discussion

This work demonstrated the usefulness of publicly available analysis tools to understand the physical

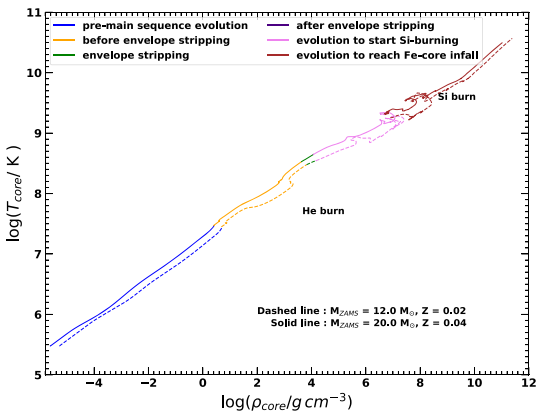

Figure 7. Variation of core temperature with core density as the models evolve through various phases on the HR diagram. Notice the very high core temperature and core density of the order of 10^{10} K and 10^{10} g cm^{-3}, respectively, towards the last evolutionary phases. Such high core temperatures and densities are indicative of the arrival of the core–collapse phase.

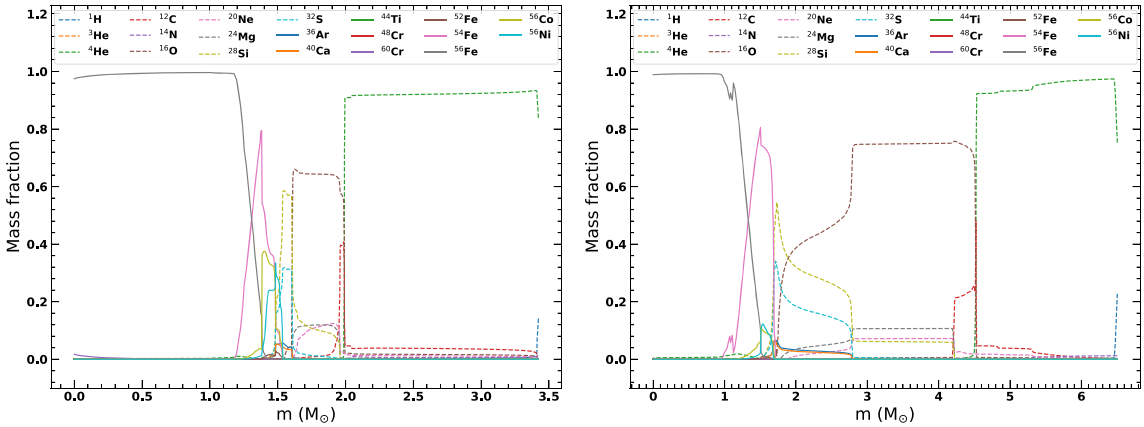

Figure 8. Mass fraction of various elements in the stellar interiors near the onset of core–collapse. Both the models show very high mass fraction of ^{56}Fe in the core, which is indicative of the arrival of the core–collapse phase. Left: The mass fraction of various elements near the arrival of the core–collapse phase of a 12 $M_{\odot}$ ZAMS progenitor with metallicity $Z = 0.02$. Right: The mass fraction of various elements near the arrival of the core–collapse phase of a 20 $M_{\odot}$ ZAMS progenitor with metallicity $Z = 0.02$.

and chemical properties of a sub-set of CCSNe and their possible progenitors. We used publicly available data as inputs to MOSFiT. Utilizing these data, MOSFiT provided various physical and chemical properties of CCSNe for assumed progenitor stars along with explosion epochs and range of required temperatures, velocities, ejecta mass, opacity, etc. Further, based on these observed properties, a certain ZAMS mass progenitors could be chosen as the possible progenitors of these CCSNe and their hydrodynamic simulations could be performed to shed light on the physical structure and required chemical engineering. The findings of the present studies can be summarized as mentioned below:

(1) With the help of MOSFiT, we fit the multi-band light curves of four H-stripped CCSNe namely, SN2009jf, iPTF13bvn, SN2015ap and SN2016bau. The parameters obtained through MOSFiT fittings were compared to those available in the literature. We demonstrated the usefulness of MOSFiT and how it could be used with an extensive data set to constrain various physical parameters more realistically.

(2) In the later part of this study, we demonstrated the importance of MESA to understand the physical and chemical properties of possible progenitors. MESA proved to be an excellent tool to study stellar evolution. In this work, we performed the hydrodynamic simulations of two progenitor models having ZAMS masses of 12 $M_{\odot}$ and 20 $M_{\odot}$, which could serve as the possible progenitors of the four H-stripped CCSNe considered for the present study. We studied the evolutions of these models on HR diagram as they evolved through various phases throughout their lifetime. Further, we studied the variation of the chemical composition inside the stellar interior as the models evolved on the main-sequence and reached the stage of He-burning termination in the core. It was noticed that as the model evolved on the main-sequence and reached the stage of termination of He-burning in the core, the stellar interior composed of more and more of heavier metals.

(3) Further, we studied the variation of $\rho_{\rm core}$ and $T_{\rm core}$ as the models evolved from PMS up to the stages, where their cores undergo core–collapse. The $\rho_{\rm core}$ and $T_{\rm core}$ reached in excess of 10^{10} g cm^{-3} and 10^{10} K in the late evolutionary stages marking the onset of core–collapse.

(4) As another piece of evidence, we also studied the mass fractions of various elements in the stellar interiors. We found out that during the last evolutionary stages, the central regions of the stellar models are mainly composed of inert ^{56}Fe, marking the arrival of core–collapse stage.

(5) As a next step, the output of MESA models on the verge of the onset of core–collapse could be provided as input to other explosion codes capable of simulating synthetic stellar explosions. The outputs obtained through such simulations could be compared to actual SNe properties and to understand new types of transients in near future.

5. Conclusions

In this work, we demonstrated the significance of MOSFiT and MESA to understand the physical and chemical properties of H-stripped CCSNe, particularly type Ib. MOSFiT is used the fit the multi-band light curves of SNe by taking into account default powering mechanisms. The fitting results provide various physical properties including SN temperature, velocity, opacity, ejecta mass, explosion epochs, etc. Depending on the high or low ejecta mass, ZAMS progenitors of different initial masses could be modeled. Also, the variations in opacity, explosion epochs and photospheric velocities are highly sensitive to SN light curves. Thus, parameters obtained using MOSFiT could serve as initial guesses for the progenitor models using MESA that later explode synthetically to give SNe light curves and photospheric velocities. So, based on these properties, stars of certain ZAMS mass range can be modeled to depict as possible progenitors of CCSNe using MESA and can be evolved from PMS up to the onset of core–collapse using MESA. The snapshots of various physical and chemical properties can be obtained from MESA outputs, which are extremely essential to understand the stellar properties of possible progenitors of CCSNe. Thus, our studies display how publicly available analysis tools can be used to remove the shear dependency on unpublished data to extract useful scientific information about a variety of transients and to understand related aspects of nuclear astrophysics, a broader and interdisciplinary emerging research area.

Additional softwares

NumPy (Harris *et al.* 2020), Matplotlib (Caswell *et al.* 2021), mesaPlot (Wise 2019), Mesa Reader (Bill & Josiah 2017), TULIPS (Laplace 2021, 2022).

Acknowledgements

We are thankful to the referee for providing valuable comments that were highly helpful in improving the manuscript further. AA acknowledges funds and assistance provided by the Council of Scientific & Industrial Research (CSIR), India with file no. 09/948(0003)/2020-EMR-I. We further acknowledge that the high performance computing facility at ARIES played extensive role in carrying out the simulations performed in this work. RG and SBP acknowledge the financial support of ISRO under AstroSat archival data utilization program (DS_2B-13013(2)/1/2021-Sec.2).

References

Aryan A., Pandey S. B., Zheng W., *et al.* 2021a, Monthly Notices of the Royal Astronomical Society, 505, 2530

Aryan A., Pandey S. B., Kumar A., *et al.* 2021b, RMxAC, 53, 215

Aryan A., Pandey S. B., Yadav A. P., Gupta R., Tiwari S. N. 2022a, JApA, 43, 2. https://doi.org/10.1007/s12036-021-09784-6

Aryan A., Pandey S. B., Zheng W., *et al.* 2022b, MNRAS, tmp.https://doi.org/10.1093/mnras/stac2326

Bersten M. C., Benvenuto O. G., Folatelli G., *et al.* 2014, AJ, 148, 68. https://doi.org/10.1088/0004-6256/148/4/68

Bill Wolf, Josiah Schwab 2017, wmwolf/py–mesa–reader: Interact with MESA Output (0.3.0). Zenodo. https://doi.org/10.5281/zenodo.826958

Bisnovatyi-Kogan G. S., Moiseenko S. G., Ardelyan N. V. 2018, PAN, 81, 266

Cao Y., Kasliwal M. M., Arcavi I., *et al.* 2013, The Astrophysical Journal, 775, L7

Caswell T. A., Droettboom M., Lee A., *et al.* 2021, zndo

Chatzopoulos E., Wheeler J. C., Vinko J., Horvath Z. L., Nagy A. 2013, The Astrophysical Journal, 773, 76. https://doi.org/10.1088/0004-637X/773/1/76

Couch S. M., Wheeler J. C., Milosavljević M. 2009, The Astrophysical Journal, 696, 953

Dessart L., Hillier D. J., Li C., *et al.* 2012, Monthly Notices of the Royal Astronomical Society, 424, 2139

Eldridge J. J., Langer N., Tout C. A. 2011, Monthly Notices of the Royal Astronomical Society, 414, 3501

Eldridge J. J., Fraser M., Maund J. R., Smartt S. J. 2015, Monthly Notices of the Royal Astronomical Society, 446, 2689. https://doi.org/10.1093/mnras/stu2197

Eldridge J. J., Maund J. R. 2016, Monthly Notices of the Royal Astronomical Society, 461, L117

Filippenko A. V. 1988, AJ, 96, 1941

Filippenko A. V., Matheson T., Ho L. C. 1993, The Astrophysical Journal Letters, 481, L89

Filippenko A. V. 1997, ARA&A, 35, 309

Garry G. 2004, Science, 304, 1915. https://doi.org/10.1126/science.1100370

Gaskell C. M., Cappellaro E., Dinerstein H. L., *et al.* 1986, The Astrophysical Journal, 306 L77

Groh J. H., Maynet G., Georgy C., Ekstrom S. 2013, A&A, 558, A131

Groh Jose H. 2017, Phil. Trans. R. Soc. A., 375, 20170219. https://doi.org/10.1098/rsta.2017.0219

Guillochon J., Parrent J., Kelley L. Z. 2017, The Astrophysical Journal, 835, 64. https://doi.org/10.3847/1538-4357/835/1/64

Guillochon J., Nicholl M., Villar V. A., *et al.* 2018, The Astrophysical Journal Supplement, 236, 6. https://doi.org/10.3847/1538-4365/aab761

Harris C. R., Millman K. J., van der Walt S. J., *et al.* 2020, Nature, 585, 357. https://doi.org/10.1038/s41586-020-2649-2
Henyey L., Vardya M. S., Bodenheimer P. 1965, The Astrophysical Journal, 142, 841
Herwig F. 2000, Astronomy & Astrophysics, 360, 952
Kippenhahn R., Ruschenplatt G., Thomas H.-C. 1980, Astronomy & Astrophysics, 91, 175
Könyves-Tóth R., Vinkó J., Ordasi A., *et al.* 2020, The Astrophysical Journal, 892, 121K
Kumar A., Pandey S. B., Singh A., *et al.* 2021, 2111.13018
Langer N., El Eid M. F., Fricke K. J. 1985, Astronomy & Astrophysics, 145, 179
Laplace E. 2021, ascl.soft. ascl:2110.004
Laplace E. 2022, A&C, 38, 10.0516. https://doi.org/10.1016/j.ascom.2021.100516
Liccardo V., Malheiro M., Hussein M. S., Carlson B. V., Frederico T. 2018, EPJA, 54, 221. https://doi.org/10.1140/epja/i2018-12648-5
Maoz D., Mannucci F., Nelemans G. 2014, ARA&A, 52, 107
Meyer M., Petrushevska T., Fermi-LAT Collaboration 2020, Phys. Rev. Lett., 124, 231101. https://doi.org/10.1103/PhysRevLett.124.231101
Muller B. 2017, IAUS, 329, 17
Nadyozhin D. K. 1994, The Astrophysical Journal Supplement, 92, 527. https://doi.org/10.1086/192008
Nicholl M., Guillochon J., Berger E., 2017, The Astrophysical Journal, 850, 55. https://doi.org/10.3847/1538-4357/aa9334
Pandey S. B., Yadav R. K. S., *et al.* 2018, BSRSL, 87, 42
Pandey S. B., Kumar A., Kumar B., *et al.* 2021, Monthly Notices of the Royal Astronomical Society, 507, 1229
Paxton B., Bildsten L., Dotter A., *et al.* 2011, The Astrophysical Journal Supplement, 192, 3
Paxton B., Cantiello M., Arras P., *et al.* 2013, The Astrophysical Journal Supplement, 208, 4
Paxton B., Marchant P., Schwab J., *et al.* 2015, The Astrophysical Journal Supplement, 220, 15
Paxton B., Schwab J., Bauer E. B., *et al.* 2018, The Astrophysical Journal Supplement, 234, 34
Paxton B., Smolec R., Schwab J., *et al.* 2019, The Astrophysical Journal Supplement, 243, 10
Piran, Tsvi, Nakar, Ehud, Mazzali, Paolo, Pian, Elena 2019, The Astrophysical Journal Letters, 871, L25
Prentice S. J., Ashall C., James P. A., *et al.* 2019, Monthly Notices of the Royal Astronomical Society, 485, 1559
Sahu D. K., Gurugubelli U. K., Anupama G. C., Nomoto K. 2011, Monthly Notices of the Royal Astronomical Society, 413, 2583. https://doi.org/10.1111/j.1365-2966.2011.18326.x
Smartt S. J. 2009, ARA&A, 47, 63
Valenti S., Fraser M., Benetti S., *et al.* 2011, Monthly Notices of the Royal Astronomical Society, 416, 3138. https://doi.org/10.1111/j.1365-2966.2011.19262.x
Van Rossum D. R., Kashyap R., Fisher R., *et al.* 2016, The Astrophysical Journal, 827, 128
Villar V. A., Berger E., Metzger B. D., Guillochon J. 2017, The Astrophysical Journal, 849, 70. https://doi.org/10.3847/1538-4357/aa8fcb
Wise, Michael 2019, MESAplot is a graphical user interface for plotting MESA data with python. Zenodo. https://doi.org/10.5281/zenodo.2619274
Woosley S. E., Janka T. 2005, Nature Physics, 1, 147
Yoon S.-C., Woosley S. E., Langer N. 2010, The Astrophysical Journal, 725, 940